# Unveiling the pathogenesis of non-alcoholic fatty liver disease by decoding biomarkers through integrated single-cell and single-nucleus profiles

Wenfeng Ma [1,2,3,4], Xin Zhong [1,4], Benqiang Cai [1,4], Mumin Shao [6,7], Xuewen Yu [6,7], Minling Lv [1,4], Shaomin Xu [1,4], Bolin Zhan [1,4], Qun Li [1,4], Mengqing Ma [1,4], Mikkel Brejnholt Kjær [5,8], Jinrong Huang [2]*, Yonglun Luo [2,3]*, Henning Grønbæk [5]*, Lin Lin [2,3]*

1 Department of Liver Disease, Shenzhen Traditional Chinese Medicine Hospital, Shenzhen, Guangdong 518033, China.
2 Department of Biomedicine, Aarhus University, Aarhus, Denmark.
3 Steno Diabetes Center Aarhus, Aarhus University Hospital, Aarhus, Denmark.
4 Department of Liver Disease, The Fourth Clinical Medical College of Guangzhou University of Chinese Medicine, Shenzhen, 518033, China.
5 Department of Hepatology and Gastroenterology, Aarhus University Hospital, Aarhus, Denmark.
6 Department of Pathology, Shenzhen Traditional Chinese Medicine Hospital, Shenzhen, Guangdong 518033, China.
7 Department of Pathology, The Fourth Clinical Medical College of Guangzhou University of Chinese Medicine, Shenzhen, 518033, China.
8 Department of Clinical Medicine, Aarhus University, Aarhus, Denmark.
* = corresponding author

## Highlights

- Integrated single-cell and single-nucleus profiles from 82 liver and PBMC specimens comprising NAFLD patients and healthy controls with increasing

severity were utilized to unveil the NAFLD pathogenesis through decoding candidate biomarkers of NAFLD.

- In cell-level observations, we decoded 16 up-regulated and 22 down-regulated secreting genes previously identified as associated with increasing NAFLD severity in the liver RNA-seq and plasma proteomics data.
- QSOX1, enriched in fibroblasts, and IL1RAP, enriched in hepatocytes, have been further validated and interpreted in integrated single-cell and single-nucleus profiles for their potential to predict NAFLD severity.
- The analysis of intercellular crosstalk, focusing on secreted signaling from our previously identified candidate biomarkers sourced from secreted genes, highlighted the IL1B-(IL1R1+IL1RAP) pathway between liver monocytes and hepatocytes/cholangiocytes. This suggests that this pathway might be a potential reason for the observed downregulation of IL1RAP in NAFLD liver.

## Abstract

**Background and Aims:** Non-alcoholic fatty liver disease (NAFLD) is a heterogenous liver disease encompassing pathological changes ranging from simple steatosis, inflammation and fibrosis to cirrhosis. To further unravel NAFLD pathogenesis, we aimed to decode the candidate NAFLD biomarkers associated with NAFLD severity using publicly available single-cell RNA sequencing (scRNA-seq) and single-nucleus RNA sequencing (snRNA-seq) data.

**Methods:** Seurat v5 and anchor-based reciprocal principal components analysis (RPCA) integration were performed to integrate and analyze the scRNA-seq and snRNA-seq data of 82 liver and Peripheral Blood Mononuclear Cell (PBMC) specimens from NAFLD patients and healthy controls to decode the candidate NAFLD biomarkers generated previously. Using the 'CellChat' R package, we analyzed ligand-receptor interactions of our candidate biomarkers from secreted genes to understand their signaling crosstalk and implications in NAFLD's biological processes.

**Results:** We generated a database (https://dreamapp.biomed.au.dk/NAFLD-scRNA-seq/) to present the NAFLD pathogenesis by analyzing integrated scRNA-seq and snRNA-seq data. Through cell-level decoding, we discovered the expression distribution of the candidate biomarkers associated with NAFLD severity. The analysis of ligand-receptor pairs in NAFLD liver and PBMC data suggests that the IL1B-(IL1R1+IL1RAP) interaction between liver monocytes and hepatocytes/cholangiocytes may explain the correlation between NAFLD severity and IL1RAP down-regulation.

**Conclusions:** We confirmed a strong correlation between liver QSOX1/IL1RAP concentrations and NAFLD severity at the cellular level. Additionally, our analysis of comprehensive data unveiled new aspects of NAFLD pathogenesis and intercellular communication through the use of scRNA and snRNA sequencing data. (ChiCTR2300073940).

## Lay Summary

We integrated single-cell RNA sequencing (scRNA-seq) and single-nucleus RNA sequencing (snRNA-seq) data to unravel non-alcoholic fatty liver disease (NAFLD) pathogenesis. We decoded candidate biomarkers associated with NAFLD progression, which were previously screened from RNA sequencing (RNA-seq) data of 625 liver samples with a novel gene clustering method. A new version of the R package ''Seurat v5' and anchor-based reciprocal principal components analysis (RPCA) integration were performed to process and integrate scRNA-seq and snRNA-seq data of 82 liver and Peripheral Blood Mononuclear Cell (PBMC) specimens from NAFLD patients and healthy controls. The research delved deeper into the cellular expression patterns of the candidate biomarkers and examined the intercellular communication of their secreted signaling.

## Graphical abstract

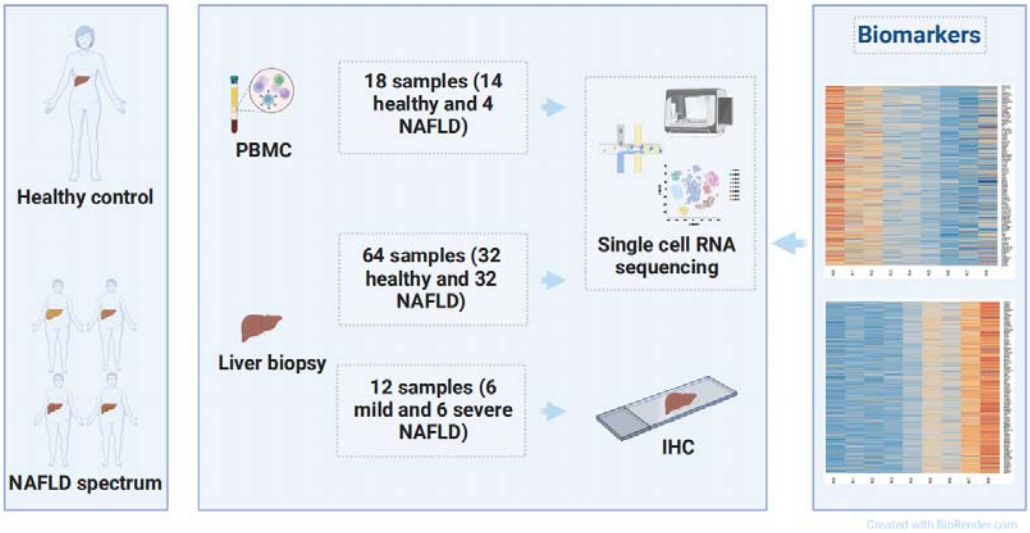



## Keywords

Non-alcoholic fatty liver disease, pathogenesis, single-cell and single-nucleus RNA sequencing data integration, quiescin sulfhydryl oxidase 1, interleukin-1 receptor accessory protein

## Introduction

Non-alcoholic fatty liver disease (NAFLD) is a multifaceted disease representing a spectrum from Non-alcoholic Fatty Liver (NAFL) of simple steatosis, non-alcoholic steatohepatitis (NASH) to NASH-induced fibrosis and cirrhosis (1, 2). As the global prevalence of NAFLD reached 38.0%, the upward trend in NAFLD and NASH-related liver cancer balanced the declining tendency of virally-caused hepatocellular carcinoma (3-5). Despite the noteworthy advancements in NAFLD research, the lack of FDA-approved treatments underscores the need for a systematic study to understand its pathogenesis (6, 7).

The advent of transcriptomics, specifically single-cell RNA sequencing (scRNA-seq) and single-nucleus RNA sequencing (snRNA-seq) has triggered a paradigm shift in our comprehension of biological processes, cellular diversity, and the intricacies of physiological and disease states (8). These groundbreaking technologies allow us to examine gene expression at the cell level, significantly enhancing our understanding of various aspects of life sciences (9, 10). In 2019, Xiong et al. applied scRNA-seq to reveal the cellular heterogeneity of NAFLD, identifying key cell types and crosstalk during disease progression (11). Tamburini et al. focused on liver lymphatic endothelial cells (LECs) and observed the activation of the IL13 pathway in LECs of NASH patients (12). In 2020, Ramachandran et al. utilizing single-cell transcriptomics, resolved human liver tissue and blood samples of patients with cirrhosis and healthy controls, identifying new pathogenic subpopulations and providing the markers of cell subtypes (13). In 2021, Deczkowska and colleagues discovered an abundance and activation of type 1 conventional dendritic cells (cDC1) in both NAFLD and NASH conditions with scRNA-seq. They further highlighted XCR1+ cDC1 as a significant contributor to liver pathology in NASH (14). Recently, Wang et al. interpreted NASH-associated hepatic stellate cells (HSCs) with snRNA-seq and uncovered an autocrine HSC signaling circuit that emerged in advanced fibrosis (15). These studies underscore the immense potential of transcriptomics application in NAFLD research

120 for finding molecular signatures and pathways that could guide the development of
121 diagnosis and therapeutics for NAFLD.
122
123 Recently, we demonstrated that Quiescin sulfhydryl oxidase 1 (QSOX1) and
124 Interleukin-1 receptor accessory protein (IL1RAP) hold potential as indicators of liver
125 disease severity in NAFLD patients (16). QSOX1, a flavin-linked enzyme that facilitates
126 disulfide bond formation within the secretory structures of mammalian cells, is
127 expelled into the extracellular matrix (ECM) and blood as an independent protein
128 through the standard secretory pathway, encompassing the Golgi apparatus,
129 secretory vesicles, and the plasma membrane. Furthermore, it is notably amplified
130 and released from fibroblasts that are actively synthesizing ECM precursors (15-17).
131 On the other hand, IL1RAP, a member of the IL-1 receptor family, is ubiquitously
132 present but shows high levels in the liver, placenta, and white blood cells, according
133 to databases such as NCBI. This protein plays a critical role in inflammation and is
134 implicated in the initiation and progression of cancer. Studies suggested that both
135 QSOX1 and IL1RAP hold promise as potential biomarkers of NAFLD or obesity (17,
136 18).
137
138 In 2022, Hao's team unveiled Seurat v5, featuring a 'bridge integration' technique
139 designed to merge single-cell datasets from diverse molecular domains and various
140 measurement modalities. Employing concepts from 'dictionary learning' within the
141 field of representation learning, this method is highly scalable and ideal for handling
142 expansive datasets of millions of cells. It has wide applicability across different
143 technologies and molecular modalities, making it valuable for large research
144 consortia with existing single-cell RNA-seq databases. Additionally, the approach
145 shows potential in the identification and comprehensive study of rare cellular
146 populations. Overall, the introduction of bridge integration in Seurat v5 is poised to
147 make a significant impact on the advancement of single-cell research (19). Compared
148 to its predecessor (20), Seurat v5 enhanced its capacity for large-scale data
149 integration and facilitated a more comprehensive analysis of the cellular and nuclear

150 transcriptomic landscapes. With Seurat v5, we aimed to use publicly available
151 scRNA-seq and snRNA-seq data to decode the candidate NAFLD biomarkers we have
152 previously screened for unraveling NAFLD pathogenesis.
153
154 Understanding global cellular interactions necessitates precise representation and
155 analysis of cell-to-cell signaling pathways. "CellChat" serves as a tool, crafted to
156 extract and evaluate intercellular communication networks from sc- and snRNA-seq
157 data (21). It identifies primary signaling pathways for cells, decoding their
158 coordinated actions through network analyses and pattern detection methods. Using
159 manifold learning and quantitative assessments, CellChat classifies signaling routes
160 and differentiates between universal and context-specific pathways across diverse
161 datasets. Consequently, it aids in revealing novel intercellular communications and in
162 building communication blueprints for a range of tissues (22).
163

164 ## Materials and methods

165 **Single-cell and Single-nucleus RNA-seq Data Analysis**

166 1. Data Collection

167 The scRNA-seq and snRNA-seq data from human liver and Peripheral Blood
168 Mononuclear Cell (PBMC) of NAFLD and healthy controls were collected from the
169 NCBI GEO (until June 2023). Only datasets generated with 10x Genomics Single-Cell
170 Reagent Kit were included.
171

172 2. Data Alignment

173 The FASTQ-formatted data were downloaded and converted into feature, barcode
174 and matrix with the human GRCh38 genome using 'cellranger' (cellranger-6.1.2). For
175 snRNA-seq, intron was included for quantification (23). The doublets were removed
176 with the R package 'DoubletFinder' (DoubletFinder-2.0.3) for each sample.
177

178 3. Data Normalization and Clustering

With the R package 'Seurat V5' (Seurat 4.9.9.9042) (https://satijalab.org/seurat/articles/seurat5_integration.html), the datasets were integrated and processed using the anchor-based reciprocal principal components analysis (RPCA) method. After normalization and batch correction, the scRNA-seq and snRNA-seq data underwent unsupervised clustering.

For normalization, the 'LogNormalize' method was utilized with a default scale factor of 10,000, and subsequent feature identification and data scaling were done by default. The scaled data was then subjected to Principal Component Analysis (PCA) with a default setting of computing and storing 50 Principal Components (PCs). To perform integration in low-dimensional space, we selected the anchor-based RPCA integration method, which aimed to co-embed shared scRNA-seq and snRNA-seq library types across batches, yielding a dimensional reduction (integrated.rpca).

For cell clustering, a shared nearest neighbor (SNN) modularity optimization-based algorithm was employed, with the dimensions of reduction set to 1:15 and the resolution parameter set to 0.2 (liver) and 0.1 (PBMC).

4. Cell Type Annotation and Data Analysis

We annotated liver and PBMC clusters with canonical markers by manually curated the information to enhance the accuracy of gene annotation. To gain a more nuanced understanding of transcriptomic variations, we further segmented certain cell types in additional supplementary files. This enabled us to identify subtype-specific differences in both healthy and NAFLD conditions. We then compared the expressions of potential NAFLD biomarkers across multiple clustering methodologies and depicted the results on distinct UMAP plots.

5. Cell Communication Analysis

The sc- and snRNAseq data of NAFLD liver and PBMC were merged together and RPCA integrated before normalization. A Seurat object with a new assay of 5,000

209 cells in each cell type in a tissue was subsetted. The R package 'CellChat' (CellChat
210 1.6.1) was utilized to analyze the data. We refined the CellChatDB database to
211 include only interactions involving secreted signaling, as the candidate NAFLD
212 biomarkers originate from genes that are secreted.
213
214 6. Database Construction
215 To visualize gene expression variation during the development of NAFLD severity at
216 the cell level, we generated a NAFLD sc- and snRNA-seq database (NAFLD-DB) using
217 the tool 'ShinyCell'. (https://github.com/SGDDNB/ShinyCell). This database was
218 deployed at https://dreamapp.biomed.au.dk/NAFLD-scRNA-seq/.
219
220 **Validation of QSOX1 and IL1RAP as Biomarkers in NAFLD at the Liver Cell Level**
221 1. Study Design
222 Our objective was to confirm the *QSOX1* and *IL1RAP* gene expression in cells of
223 different severity of NAFLD. To address this question, we performed
224 immunohistochemical staining (IHC) for liver QSOX1/IL1RAP on a group of NAFLD
225 patients from Shenzhen Traditional Chinese Medicine Hospital, China (SZTCMH).
226 Details of this cohort have been provided previously (16).
227
228 2. Human Samples and IHC
229 For IHC, we collected 12 fixed liver tissues from archived histological samples at
230 SZTCMH between 2014 and 2023, and details were in our earlier study (16).
231
232 3. Statistical Analysis
233 The significance for all statistical tests was two-sided, with $P < 0.05$. All data analysis
234 was presented in the plots using R-4.3.1. Statistical analysis in the Violin plots was
235 performed with Wilcoxon rank sum test to assess differences between unpaired
236 groups.
237

238 ## Results

239 **Alignment of ScRNA-seq and snRNA-seq Data**

240 We incorporated twelve datasets (GSE122083, GSE125188, GSE136103, GSE144430,
241 GSE159977, GSE169446, GSE175793, GSE179886, GSE182159, GSE189539,
242 GSE212837 and GSE217235) into our study. The scRNAseq and snRNA-seq data
243 encompass liver and PBMC samples of both healthy controls and patients with
244 NAFLD (**Supplementary Table 1**). The detailed information regarding the data
245 alignment was presented in the **Supplementary Table 2.**

246

247 By employing RPCA integration, we achieved precise comparative analyses across
248 single-cell and single-nucleus sequencing datasets. To address batch effects arising
249 from diverse sequencing technologies and studies involving various experimental
250 batches, donors, and conditions, we conducted integration and normalization, as
251 depicted in **Figure 1A**. After filtering out doublets, the dataset was refined, resulting
252 in a total of 427,787 liver cells (including 214,795 healthy cells and 212,992 NAFLD
253 cells) and 122,238 PBMC cells (including 92,319 healthy cells and 29,919 NAFLD cells)
254 available for subsequent analysis.

255

256 **The Effectiveness of Integration and Normalization on Liver Transcriptome Profiles**

257 PCA demonstrated the effectiveness of the RPCA integration and normalization
258 process in eliminating noticeable batch effects of liver transcriptome profiles
259 compared to the unintegrated UMAP, as depicted in **Figure 1B and 1C**. Moreover,
260 sample separation was not primarily driven by health/NAFLD group or library type, as
261 indicated in **Figure 1D and 1E**. Instead, cell type emerged as the primary factor
262 influencing transcriptome profiles, as illustrated in **Figure 1F**.

263

264 **Unsupervised Clustering and Annotation of Liver Cells and Nuclei Data**

265 Initially, we categorized all 427,787 liver cells into 12 distinct cell types using gene
266 markers. The identified cell types were annotated using signatures of known

canonical markers (**Figure 2A, B; Supplementary Table 3**).

**Tracing the Cellular Origins of Promising Biomarkers for Liver NAFLD Severity**

In our previous study (16), we pinpointed key genes that are significantly involved in the advancement of NAFLD. Specifically, we discovered 16 genes, including A2M, C7, COL6A3, COLEC11, ENPP2, FBLN1, FBN1, FCGBP, IGFBP6, LCN2, LUM, MMP2, PAPLN, PTGDS, QSOX1, and VWF, that exhibited elevated secretory activity correlating with the severity of NAFLD. On the other hand, we also identified another set of 22 genes, namely AZGP1, C1RL, C4BPA, C6, C8B, CFHR3, CNDP1, F2, GC, HP, HPR, IL1RAP, ITIH1, ITIH2, ITIH4, KLKB1, PON3, SERPINA10, SERPINC1, SERPING1, SMPDL3A, and TTR, that showed reduced secretory activity, also in relation to the severity of the condition. These particular genes were not only implicated through RNA-seq data but were also corroborated by proteomics datasets. The correlation was such that the expression patterns of these genes seemed to escalate or diminish in tandem with increasing NAFLD severity. We investigated how these genes contribute to NAFLD pathogenesis, and why their particular expression patterns are so closely associated with the progression of NAFLD.

Delving into the intricate cellular milieu, the expression profiles of these potential biomarkers were meticulously examined across diverse liver cell categories. It was observed that the HSC/MFB cellular contingent distinctly exhibited pronounced expression levels of C7, COL6A3, FBN1, and QSOX1 compared to other cellular phenotypes. Intriguingly, these molecular markers were conspicuously prevalent in NAFLD-afflicted cohorts over their healthy counterparts (**Figure 2C**). In light of the overwhelming majority of hepatocytes in hepatic architecture, significant expression of IL1RAP, ITIH2, TTR, and SERPINA10 was ascertained in these cells, spanning all identified subtypes. This expression spectrum was notably skewed towards the healthy clusters versus NAFLD groups, intimating a palpable downregulation at the holistic hepatic expression matrix (**Figure 2D**).

297 Cutting-edge developments in medical science have clarified the primary source of
298 myofibroblasts, identifying hepatic stellate cells (HSCs) as their main origin (24, 25).
299 Functioning as lipid storage entities, HSCs share considerable similarity with
300 adipocytes, or fat cells, particularly when the liver is functioning optimally (26). This
301 newfound insight broadens our understanding of liver diseases, including liver
302 fibrosis and cirrhosis, where myofibroblasts play a significant role. Interestingly, the
303 elevated levels of QSOX1, which is enriched in the HSC/MFB, correlate with both the
304 NAS score and fibrosis score, offering a potential biomarker for NAFLD severity.
305
306 A more detailed exploration of the HSC/MFB clustering, and annotation using
307 canonical markers has revealed two distinct subsets: hepatic stellate cells and
308 myofibroblasts (**Figure 2E, F; Supplementary Table 3**). Within this context, QSOX1
309 manifested heightened expression within the NAFLD subset of HSC (**Figure 2G**). In
310 contrast, IL1RAP and CFHR3, bearing the torch for the loftiest expression within
311 hepatocytes amongst all subtypes, evinced diminished expression within the NAFLD
312 demographic compared to its healthier cohort (illustrated in **Figure 2H**).
313
314 In a supplementary validation, liver biopsies sourced from patients with varying
315 NAFLD severity were subjected to IHC in our antecedent study (16). Conclusive
316 findings reinforced that QSOX1 resonates with heightened expression specifically in
317 HSC/MFB cells of severe NAFLD patients (**Figure 2I**), while IL1RAP's expression was
318 attenuated in hepatocytes of these patients as seen in **Figure 2J** (16).
319
320 **The Effectiveness of Integration and Normalization on PBMC Transcriptome Profiles**
321 To explore the expression of biomarkers in PBMC between NAFLD patients and
322 healthy controls, we tracked their expression variations using RPCA integrated
323 scRNA-seq data. The results from PCA showed that normalization successfully
324 mitigated discernible batch effects compared to the unintegrated data, as shown in
325 **Figure 3A and B**. The primary factors driving sample differentiation were not the
326 health and NAFLD group, as depicted in **Figure 3C**. Instead, the cell type surfaced as

327 the primary determinant impacting transcriptome profiles, as illustrated in **Figure 3D**.

328

329 **Unsupervised Clustering Identifies Clusters of PBMC Cells**

330 We first clustered all the 122,238 PBMC cells into 6 cell types, and the identified cell
331 types were annotated using signatures of known canonical markers (**Figure 3E, F;**
332 **Supplementary Table 3**).

333

334 **Tracing the Cellular Origins of Promising Biomarkers for NAFLD severity in PBMC**

335 We identified 16 genes that are up-regulated (A2M, C7, COL6A3, COLEC11, ENPP2,
336 FBLN1, FBN1, FCGBP, IGFBP6, LCN2, LUM, MMP2, PAPLN, PTGDS, QSOX1, VWF) and
337 22 that are down-regulated (AZGP1, C1RL, C4BPA, C6, C8B, CFHR3, CNDP1, F2, GC, HP,
338 HPR, IL1RAP, ITIH1, ITIH2, ITIH4, KLKB1, PON3, SERPINA10, SERPINC1, SERPING1,
339 SMPDL3A, TTR) with increasing severity of NAFLD, as evidenced by both RNA-seq and
340 proteomics data. In PBMC, QSOX1 and IL1RAP have the highest expression levels in
341 Natural killer cells (NK cells) across all subtypes. Interestingly, healthy individuals
342 showed higher expression of these genes than those with NAFLD (**Figure 3G, H**).
343 Nonetheless, the baseline expression levels of these genes in PBMC were too faint to
344 support a significant comparison. The low expression within PBMC may not affect
345 their detectability and proportional concentrations in plasma. Even when a gene
346 exhibits varied expression in a distinct cell type or tissue, it's not a given that there
347 will be discernible differences in broader systems like plasma, especially when the
348 initial expression is inherently low (**Figure 3I, J**).

349

350 **The intercellular crosstalk in the liver and PBMC of NAFLD patients and healthy**
351 **controls revealed by integrated sc- and snRNAseq data analysis**

352 Since our candidate biomarkers were derived from secreted genes, it was essential to
353 delve deeper into the communication mechanisms of these genes. We utilized the
354 'CellChat' R package to analyze the ligand-receptor interactions, enabling us to better
355 understand the crosstalk of secreted signaling and their potential implications in the
356 biological processes of NAFLD.

357

358 The integrated RPCA analysis combined a total of 427,787 liver cells and 122,238
359 peripheral blood mononuclear cells (PBMCs). The data was then partitioned into
360 subsets comprising 5,000 cells for each cell type within the respective tissues.
361 Subsequent analysis was carried out using the 'CellChat' R package (**Figure 4A**). The
362 examination of ligand-receptor pairs of secreted signaling, which constitutes 61.8%
363 of all categories as depicted in **Figure 4B**, within the transcriptomic data from the
364 liver and PBMCs in the NAFLD group indicates a strong correlation. Specifically, the
365 interaction between IL1B-(IL1R1+IL1RAP) in liver monocytes and
366 hepatocyte/cholangiocyte may provide a convincing rationale for the correlation
367 between NAFLD severity and the down-regulated expression of IL1RAP in the liver, as
368 highlighted in **Figure 4C and F**. In our earlier research (16), we pinpointed potential
369 diagnostic markers from candidate genes by juxtaposing both up-regulated and
370 down-regulated gene clusters against the secretome database from the Human
371 Protein Atlas. Through this cross analysis, we discovered 349 genes that encode
372 secreted proteins: 249 of these genes were up-regulated, while 100 were
373 down-regulated. Of the totally 349 secreted genes, both FGFR2 and JAM3 exhibited
374 up-regulation, while ERBB3 and SDC4 were notably down-regulated. These four
375 genes are cataloged within the ligand-receptor pairs in the CellChat database, as
376 referenced in **Supplementary Table 4**. Yet, when examining the crosstalk analysis
377 derived from the sc- and snRNAseq data of NAFLD patients, only the down-regulated
378 SDC4 (ANGPTL4-SDC4) and ERBB3 (NRG1-ERBB3) emerged as significant receptors in
379 these pairs (see **Supplementary Tables 4 and 5**). The ANGPTL4-SDC4 pairing occurs
380 between liver hepatocytes and hepatocyte/cholangiocyte, as depicted in **Figures 4D**
381 **and 4G**. Similarly, the NRG1-ERBB3 interaction is evidenced between liver
382 hepatocytes and cholangiocytes, highlighted in **Figures 4E and 4G**. An accompanying
383 violin plot reveals expression patterns of the three crucial down-regulated secreted
384 genes from the crosstalk analysis. Intriguingly, Most of them are predominantly
385 found in hepatocytes, as demonstrated in **Figure 4H**. It may intricate that the
386 significant down regulation of liver gene expression in bulk RNA sequencing may

387 mostly caused by the gene variation in hepatocyts since it is the biggest population in
388 the liver. And the down-regulation may caused by the ligands acted on the receptors
389 in the hepatocytes when the NAFLD severity developed.
390

391 ## Discussion

392 The inherent complexities of NAFLD pathogenesis consistently propel scientists to
393 extend the boundaries of traditional diagnostic and investigative methodologies,
394 thus underscoring the escalating importance of genomics technology within this
395 domain. Our research RPCA integrated publicly available scRNA-seq and snRNA-seq
396 datasets to identify potential biomarkers, thereby contributing to the enhanced
397 understanding of the intricate pathogenic processes driving NAFLD (27). Using this
398 approach, we corroborated the significant correlation between the expression ratio
399 of QSOX1/IL1RAP and the severity of NAFLD at the cellular level (16). Furthermore,
400 through an analysis of the integrated large-scale scRNA and snRNA sequencing data
401 to interpret potential biomarkers, we shed light on previously undiscovered facets of
402 NAFLD pathogenesis and intercellular crosstalk.
403

404 QSOX1 and its less common variant, QSOX2, are unique among sulfhydryl oxidases
405 because they are specifically found in the Golgi apparatus of animal cells (28).
406 Studies found elevated expression of QSOX1 in quiescent fibroblasts, and it is also
407 released into the bloodstream (29, 30). QSOX1 plays a crucial role in the proper
408 construction of the ECM, particularly elements similar to the basement membrane
409 (BM) in cell culture. The BM, an ECM layer interfacing bodily cavities or blood vessels
410 with underlying stromal fibroblasts, is largely composed of elements generated by
411 fibroblasts (31). The exact reason behind QSOX1's secretion—whether due to
412 overwhelming the Golgi's retention mechanism or some specialized secretion
413 pathway—remains unclear. Our findings highlight an increased expression of QSOX1
414 in fibroblasts within NAFLD-affected liver tissue, suggesting that Golgi function in
415 fibroblasts could be a relevant focus for NAFLD research (32).

416

417 Fibrogenesis is a key driver in NAFLD progression and is chiefly managed by
418 specialized cells called myofibroblasts (33, 34). While these cells are not present in a
419 healthy liver, they can quickly develop following liver damage. Emerging research has
420 established that these myofibroblasts predominantly originate from hepatic stellate
421 cells (HSCs) (24, 25) , which act mainly as lipid storage cells and bear resemblance to
422 fat cells, or adipocytes, under healthy conditions (26).

423

424 In our previous article (16), the GO analysis revealed significant enrichment of the
425 up-regulated genes involved in the fibrosis-related process, such as ECM organization.
426 Similar to QSOX1 in terms of expression pattern and location, COL6A3 is associated
427 with liver fibrosis and also plays a role in the ECM organization (35). Increased
428 production of ECM moieties by diverse liver cell types is tightly linked with hepatic
429 fibrosis. Research has demonstrated that adipocytes are affected by the mechanics of
430 their surrounding ECM, such as stiffness and architecture, independent of initial
431 ligand density. In response to a stiffened, modified ECM structure, adipocytes
432 enhance the expression of fibrotic genes and increase ECM deposition. This reaction
433 eventually results in a dysfunctional, fibrotic state (36, 37). This represents a
434 significant research trajectory in the ongoing investigation of NAFLD pathophysiology.

435

436 IL1RAP is a crucial co-receptor expressed in numerous tissues and cell types,
437 emphasizing its pivotal role in immune responses, cancers, and infectious diseases
438 (38). The IL1RAP serves as a subunit to the type I IL-1 receptor (IL-1RI), a specific
439 plasma membrane receptor, which facilitates the transmission of numerous
440 biological effects of the pro-inflammatory cytokine IL-1 on an array of target cells (39,
441 40). Research indicates that one of the isoforms of IL1RAP, known as the soluble
442 isoform of the IL-1 receptor accessory protein (sIL1RAP), has been found to have
443 lower levels in the plasma of obese individuals when compared to their non-obese
444 subjects (17). IL1RAP, enriched in the cytoplasm of liver cells and released into the
445 bloodstream, shows variations in expression levels that correlate with the severity of

NAFLD, as per our study. Nevertheless, its specific role in NAFLD progression remains an enigma.

CFHR3, displaying similar expression patterns and localization as IL1RAP, also warrants further investigation for its potential role in diagnosing NAFLD (30). The complementary DNAs (cDNAs) that encode CFHR3 were extracted from a human liver cDNA library. These have been located within the 'regulators of complement activation' (RCA) gene cluster situated on human chromosome 1 (41, 42). CFHR3 has been linked with some diseases, including hepatocellular carcinoma (HCC), although the underlying mechanism is still not clearly understood (43). Our research indicates that CFHR3 expression decreases in correlation with the severity of NAFLD, including both the NAS and fibrosis scores. This finding opens a new avenue of research into the pathophysiology of NAFLD.

The IL1 pathway, especially IL1B, has attracted significant attention and has been extensively researched within the realm of NAFLD (35, 44-47). IL-1β exacerbates liver steatosis, inflammation, and fibrosis by interacting with the IL-1 receptor, which is extensively expressed across various liver cell types (44). In 2021, Unamuno et al. discovered that in the liver of obese patients with NASH, there was a significant upregulation of mRNA levels for NLRP3 ($P < 0.05$) and its associated proinflammatory mediator IL1B ($P < 0.01$) (35). In 2018, Pan and colleagues showed that in NASH patients, IL-1β is primarily secreted by Kupffer cells, which are a type of monocyte in the liver. This secretion is driven by the activation of the NLRP3 inflammasome, stimulated by mitochondrial DNA (48). From our studies on cellular interactions within NAFLD, we have formed and to some extent validated a hypothesis that the IL-1β, when secreted, serves as a ligand affecting the receptors IL1R1 and IL1RAP in both hepatocytes and cholangiocytes. This interaction between the ligand and its receptors seems to play a crucial role in modulating the expression of IL1RAP, which is closely associated with NAFLD severity. The dynamic interplay between these cellular components provides a deeper understanding of the disease's underlying mechanisms and offers potential

avenues for NAFLD biomarkers and therapeutic interventions.

The utility of Seurat v5 in processing and integrating scRNA-seq and snRNA-seq data is apparent in our study. However, we must also acknowledge the inherent limitations of these techniques (49). Therefore, our findings must be interpreted with caution, and further confirmatory studies are required to validate the candidate biomarkers and the NAFLD pathogenesis.

Utilizing the 'CellChat' R package allowed for a streamlined analysis of the data. Given the vastness of the data, it was segmented into more digestible portions, sketching them into clusters of 5,000 cells each, ensuring a more organized scrutiny. An outstanding revelation from this analysis was the significant presence of ligand-receptor pairs of secreted signaling within the NAFLD group, which constituted a remarkable 61.8% of all categories. This prevalence underscored their crucial role in the interactions between liver and PBMC cells. The interaction of IL1B-(IL1R1+IL1RAP) between liver monocytes and hepatocyte/cholangiocyte was of particular interest, suggesting a plausible explanation for the detected decline in IL1RAP expression in the liver - a potential indicator of NAFLD severity. Referring back to our prior research, the crosstalk analysis, built on sc- and snRNAseq data from NAFLD patients, spotlighted SDC4 (in association with ANGPTL4) and ERBB3 (aligned with NRG1) as receptors of importance. The relationships between ANGPTL4-SDC4 and NRG1-ERBB3 with liver hepatocytes and hepatocyte/cholangiocytes, respectively, reflect their likely significance in the liver's cellular dynamics. This proposition is bolstered by a violin plot that vividly illustrates the expression patterns of three crucial down-regulated secreted genes from the crosstalk analysis, with hepatocytes prominently featuring as their central hub.

Syndecan-4 (SDC4) is a transmembrane protein that is glycosylated and prevalent in numerous tissues (50). Essential cellular functions such as differentiation, adhesion, migration, and prognosis are facilitated by SDC4, given its ability to bind to a variety of external molecules and engage in signal transmission (51-53).

ERBB3, or Receptor tyrosine-protein kinase erbB-3, is a membrane-associated protein from the EGFR/ERBB family of receptor tyrosine kinases. Research has shown its involvement in numerous liver conditions, including liver fibrosis (54, 55).

In conclusion, our research sheds light on the intricacies of NAFLD pathogenesis and highlights the significance of newly identified biomarkers in tracking disease progression. These insights serve as a foundation for subsequent studies delving into the molecular intricacies of NAFLD, all aiming towards enhancing disease diagnosis, management, and the outcomes of patients.

## Abbreviations

avg_log2FC, log fold-change of the average expression between the two groups; BM, basement membrane; cDC1, type 1 conventional dendritic cell; cDNAs, complementary DNAs; ECM, extracellular matrix; F, Fibrosis score; GEO, Gene Expression Omnibus; GO, Gene Ontology; GRCh37, Genome Reference Consortium Human Build 37; HCC, hepatocellular carcinoma; HSCs, hepatic stellate cells; IHC, immunohistochemistry staining; IL-1RI, type I IL-1 receptor; IL1RAP, Interleukin-1 receptor accessory protein; LECs, lymphatic endothelial cells; N, NAS score; NAFL, Non-alcoholic Fatty Liver; NAFLD, Non-alcoholic fatty liver disease; NAFLD-DB, NAFLD gene expression database; NAS, NAFLD activity scores; NASH, Non-alcoholic Steatohepatitis; NK cells, Natural killer cells; PBMC, Peripheral blood mononuclear cell; PCA, Principal components analysis; PCs, Principal Components; QSOX1, Quiescin sulfhydryl oxidase 1; RCA, regulators of complement activation; RNA-seq, RNA sequencing; RPCA, reciprocal principal components analysis; scRNA-seq, single-cell RNA sequencing; sIL1RAP, the soluble isoform of the IL-1 receptor accessory protein; SNN, shared nearest neighbor; snRNA-seq, Single-nucleus RNA sequencing; SZTCMH, Shenzhen Traditional Chinese Medicine Hospital, China; UMAP, Uniform Manifold Approximation and Projection.

## Financial support

This research was funded by the Shenzhen Sanming Project of Medicine in Shenzhen, China (grant nos. SZSM201612074).

## Authors' contributions

WFM and LL designed the study and interpreted the data. The analysis strategy has been developed by LL and WFM. WFM and LL collected, analyzed, and interpreted the data. WFM drafted the manuscript. YLL, HG, and MBK revised the manuscript. WFM and LL performed data analysis and interpretation. BQC, JRH, MLL, XZ, SMX, BLZ, QL, QH, MQM contributed to the validation of the candidate biomarkers. Technical support: LL and JRH. All authors reviewed and approved the final version of the manuscript.

## Data and code availability statement

The data that support the findings of this study are available from the corresponding author upon reasonable request.

## Conflict of interest

Henning Grønbæk has received research grants from Abbvie, Intercept, ARLA Food for Health, ADS AIPHIA Development Services AG. Consulting Fees from Ipsen, NOVO, Pfizer. Lecturer for AstraZeneca and EISAI; and on Data Monitoring Committee at CAMURUS AB. All other authors have no conflicts of interest to declare.

## Figure Legend

**Figure 1. Liver single-cell and nucleus RNA sequencing data integration**

A. Illustration of data processing.

B.Uniform Manifold Approximation and Projection (UMAP) based on the unintegrated data.

C. UMAP based on the anchor-based reciprocal principal components analysis (RPCA) integrated data.

D.UMAP based on the health and NAFLD groups after RPCA integration.

E. UMAP based on the library type after RPCA integration.

F. UMAP based on the input cell type after RPCA integration.

**Figure 2. Integrated liver transcriptome data annotation, analysis and verification**

A. Gene markers of liver cell types.

B. Total 12 distinct cell types were clustered according to the canonical markers.

C. Dot plot of 16 up-regulated secreting marker expressions in cell clusters.

D. Dot plot of 22 down-regulated secreting marker expressions in cell clusters.

E. Gene markers of HSC (hepatic stellate cell)/MFB (myofibroblast) cell types.

F. Total 2 distinct cell types were clustered according to the canonical markers.

G. Violin plot of QSOX1 gene expressions in the hepatic stellate cell and myofibroblast.

H. Violin plot of IL1RAP, CFHR3 gene expressions in the Hepatocytes.

I.Representative immunohistochemical staining (IHC) images of QSOX1 in liver biopsies from mild NAFLD patients (N0-4, F0-2) and severe NAFLD patients (N5-8, F3-4) in our previous research (16).

J. Representative IHC images of IL1RAP in liver biopsies from mild NAFLD patients (N0-4, F0-2) and severe NAFLD patients (N5-8, F3-4) in our previous research (16). Statistical testing was performed using the Wilcoxon rank sum test, with p-values shown in the plot.

**Figure 3. Tracing the Cellular Origins in Liver and PBMC Data Integration**

A. Uniform Manifold Approximation and Projection (UMAP) based on the unintegrated data.Dot plot of 16 up-regulated secreting marker expressions in cell clusters.

B. UMAP based on the anchor-based reciprocal principal components analysis (RPCA) integrated data.

C. UMAP based on the health and NAFLD groups after RPCA integration.

D. UMAP based on the input cell type after RPCA integration.

E. Gene markers of PBMC cell types.

F. Total 6 distinct cell types were clustered according to the canonical markers.

G. Dot plot of 16 up-regulated secreting marker expressions in cell clusters.

H. Dot plot of 22 down-regulated secreting marker expressions in cell clusters.

I. Violin plot of QSOX1 gene expressions in the NK cell.

J. Violin plot of IL1RAP gene expressions in the NK cell.
Statistical testing was performed using the Wilcoxon rank sum test, with p-values shown in the plot.

**Figure 4. The cell communication in the liver and PBMC transcriptomics data**
A. UMAP based on the anchor-based reciprocal principal components analysis (RPCA) integrated liver and PBMC data.
B. Ligand-receptor pairs of secreted signaling, which constitutes 61.8% of all categories.
C. The interaction between IL1B-(IL1R1+IL1RAP) in liver monocytes and hepatocyte/cholangiocyte.
D. The ANGPTL4-SDC4 pairing occurs between liver hepatocytes and hepatocyte/cholangiocyte.
E. The NRG1-ERBB3 interaction is evidenced between liver hepatocytes and cholangiocytes
F. The interaction between IL1B-(IL1R1+IL1RAP) in liver monocytes and hepatocyte/cholangiocyte.
G. The ANGPTL4-SDC4 pairing occurs between liver hepatocytes and hepatocyte/cholangiocyte.
H. Violin plot of IL1B, IL1R1, IL1RAP, ANGPTL4, SDC4, NRG1, ERBB3 gene expressions in the liver and PBMC.

## List of Supplementary Tables

https://drive.google.com/file/d/1Eji-PHKMxil246MClmnh3PZPICD-nlCA/view?usp=sharing

## Supplementary Table 1

The scRNAseq and snRNA-seq data of liver and PBMC samples.

## Supplementary Table 2

The detailed information regarding the data alignment of the scRNAseq and snRNA-seq data.

## Supplementary Table 3

The canonical markers of cell types in the liver and PBMC.

## Supplementary Table 4

The ligand-receptor pairs in the CellChat database.

## Supplementary Table 5

The pathways in the CellChat database.

639 # Reference


640 1. Loomba R, Friedman SL, Shulman GI. Mechanisms and disease consequences of nonalcoholic
641 fatty liver disease. Cell 2021;184:2537-2564.
642 2. Powell EE, Wong VW, Rinella M. Non-alcoholic fatty liver disease. Lancet 2021;397:2212-2224.
643 3. Vogel A, Meyer T, Sapisochin G, Salem R, Saborowski A. Hepatocellular carcinoma. Lancet
644 2022;400:1345-1362.
645 4. Chen Y, Wang W, Morgan MP, Robson T, Annett S. Obesity, non-alcoholic fatty liver disease and
646 hepatocellular carcinoma: current status and therapeutic targets. Front Endocrinol (Lausanne)
647 2023;14:1148934.
648 5. Younossi ZM, Golabi P, Paik JM, Henry A, Van Dongen C, Henry L. The global epidemiology of
649 nonalcoholic fatty liver disease (NAFLD) and nonalcoholic steatohepatitis (NASH): a systematic review.
650 Hepatology 2023;77:1335-1347.
651 6. Khairnar R, Islam MA, Fleishman J, Kumar S. Shedding light on non-alcoholic fatty liver disease:
652 Pathogenesis, molecular mechanisms, models, and emerging therapeutics. Life Sci 2023;312:121185.
653 7. Musso G, Saba F, Cassader M, Gambino R. Lipidomics in pathogenesis, progression and treatment
654 of nonalcoholic steatohepatitis (NASH): Recent advances. Prog Lipid Res 2023;91:101238.
655 8. Stark R, Grzelak M, Hadfield J. RNA sequencing: the teenage years. Nat Rev Genet
656 2019;20:631-656.
657 9. Andrews TS, Atif J, Liu JC, Perciani CT, Ma XZ, Thoeni C, Slyper M, et al. Single-Cell, Single-Nucleus,
658 and Spatial RNA Sequencing of the Human Liver Identifies Cholangiocyte and Mesenchymal
659 Heterogeneity. Hepatol Commun 2022;6:821-840.
660 10. Alvarez M, Benhammou JN, Darci-Maher N, French SW, Han SB, Sinsheimer JS, Agopian VG, et al.
661 Human liver single nucleus and single cell RNA sequencing identify a hepatocellular
662 carcinoma-associated cell-type affecting survival. Genome Med 2022;14:50.
663 11. Xiong X, Kuang H, Ansari S, Liu T, Gong J, Wang S, Zhao XY, et al. Landscape of Intercellular
664 Crosstalk in Healthy and NASH Liver Revealed by Single-Cell Secretome Gene Analysis. Mol Cell
665 2019;75:644-660 e645.
666 12. Tamburini BAJ, Finlon JM, Gillen AE, Kriss MS, Riemondy KA, Fu R, Schuyler RP, et al. Chronic Liver
667 Disease in Humans Causes Expansion and Differentiation of Liver Lymphatic Endothelial Cells. Front
668 Immunol 2019;10:1036.
669 13. Ramachandran P, Dobie R, Wilson-Kanamori JR, Dora EF, Henderson BEP, Luu NT, Portman JR, et
670 al. Resolving the fibrotic niche of human liver cirrhosis at single-cell level. Nature 2019;575:512-518.
671 14. Deczkowska A, David E, Ramadori P, Pfister D, Safran M, Li B, Giladi A, et al. XCR1(+) type 1
672 conventional dendritic cells drive liver pathology in non-alcoholic steatohepatitis. Nat Med
673 2021;27:1043-1054.
674 15. Wang S, Li K, Pickholz E, Dobie R, Matchett KP, Henderson NC, Carrico C, et al. An autocrine
675 signaling circuit in hepatic stellate cells underlies advanced fibrosis in nonalcoholic steatohepatitis. Sci
676 Transl Med 2023;15:eadd3949.
677 16. Ma W, Huang J, Cai B, Shao M, Yu X, Kjær MB, Lv M, et al. A novel gene-screening approach
678 reveals QSOX1/IL1RAP as promising biomarkers for the severity of non-alcoholic fatty liver disease.
679 medRxiv 2023:2023.2007.2026.23293038.

680 17. Bozaoglu K, Attard C, Kulkarni H, Cummings N, Diego VP, Carless MA, Shields KA, et al. Plasma
681 levels of soluble interleukin 1 receptor accessory protein are reduced in obesity. J Clin Endocrinol
682 Metab 2014;99:3435-3443.
683 18. Gao R, Wang J, He X, Wang T, Zhou L, Ren Z, Yang J, et al. Comprehensive analysis of endoplasmic
684 reticulum-related and secretome gene expression profiles in the progression of non-alcoholic fatty
685 liver disease. Front Endocrinol (Lausanne) 2022;13:967016.
686 19. Hao Y, Stuart T, Kowalski MH, Choudhary S, Hoffman P, Hartman A, Srivastava A, et al. Dictionary
687 learning for integrative, multimodal and scalable single-cell analysis. Nat Biotechnol 2023.
688 20. Hao Y, Hao S, Andersen-Nissen E, Mauck WM, 3rd, Zheng S, Butler A, Lee MJ, et al. Integrated
689 analysis of multimodal single-cell data. Cell 2021;184:3573-3587 e3529.
690 21. Jin S, Guerrero-Juarez CF, Zhang L, Chang I, Ramos R, Kuan CH, Myung P, et al. Inference and
691 analysis of cell-cell communication using CellChat. Nat Commun 2021;12:1088.
692 22. Fang Z, Tian Y, Sui C, Guo Y, Hu X, Lai Y, Liao Z, et al. Single-Cell Transcriptomics of Proliferative
693 Phase Endometrium: Systems Analysis of Cell-Cell Communication Network Using CellChat. Front Cell
694 Dev Biol 2022;10:919731.
695 23. Slyper M, Porter CBM, Ashenberg O, Waldman J, Drokhlyansky E, Wakiro I, Smillie C, et al. A
696 single-cell and single-nucleus RNA-Seq toolbox for fresh and frozen human tumors. Nat Med
697 2020;26:792-802.
698 24. Yang W, He H, Wang T, Su N, Zhang F, Jiang K, Zhu J, et al. Single-Cell Transcriptomic Analysis
699 Reveals a Hepatic Stellate Cell-Activation Roadmap and Myofibroblast Origin During Liver Fibrosis in
700 Mice. Hepatology 2021;74:2774-2790.
701 25. Rosenthal SB, Liu X, Ganguly S, Dhar D, Pasillas MP, Ricciardelli E, Li RZ, et al. Heterogeneity of
702 HSCs in a Mouse Model of NASH. Hepatology 2021;74:667-685.
703 26. She H, Xiong S, Hazra S, Tsukamoto H. Adipogenic transcriptional regulation of hepatic stellate
704 cells. J Biol Chem 2005;280:4959-4967.
705 27. Hundertmark J, Berger H, Tacke F. Single Cell RNA Sequencing in NASH. Methods Mol Biol
706 2022;2455:181-202.
707 28. Reznik N, Fass D. Disulfide bond formation and redox regulation in the Golgi apparatus. FEBS Lett
708 2022;596:2859-2872.
709 29. Coppock DL, Kopman C, Scandalis S, Gilleran S. Preferential gene expression in quiescent human
710 lung fibroblasts. Cell Growth Differ 1993;4:483-493.
711 30. Uhlen M, Karlsson MJ, Hober A, Svensson AS, Scheffel J, Kotol D, Zhong W, et al. The human
712 secretome. Sci Signal 2019;12.
713 31. Grossman I, Alon A, Ilani T, Fass D. An inhibitory antibody blocks the first step in the
714 dithiol/disulfide relay mechanism of the enzyme QSOX1. J Mol Biol 2013;425:4366-4378.
715 32. Ilani T, Reznik N, Yeshaya N, Feldman T, Vilela P, Lansky Z, Javitt G, et al. The disulfide catalyst
716 QSOX1 maintains the colon mucosal barrier by regulating Golgi glycosyltransferases. EMBO J
717 2023;42:e111869.
718 33. Kisseleva T, Brenner D. Molecular and cellular mechanisms of liver fibrosis and its regression. Nat
719 Rev Gastroenterol Hepatol 2021;18:151-166.
720 34. Kisseleva T. The origin of fibrogenic myofibroblasts in fibrotic liver. Hepatology
721 2017;65:1039-1043.

722 35. Unamuno X, Gomez-Ambrosi J, Ramirez B, Rodriguez A, Becerril S, Valenti V, Moncada R, et al.
723 NLRP3 inflammasome blockade reduces adipose tissue inflammation and extracellular matrix
724 remodeling. Cell Mol Immunol 2021;18:1045-1057.
725 36. Kim M, Lee C, Seo DY, Lee H, Horton JD, Park J, Scherer PE. The impact of endotrophin on the
726 progression of chronic liver disease. Exp Mol Med 2020;52:1766-1776.
727 37. Di Caprio N, Bellas E. Collagen Stiffness and Architecture Regulate Fibrotic Gene Expression in
728 Engineered Adipose Tissue. Adv Biosyst 2020;4:e1900286.
729 38. Frenay J, Bellaye PS, Oudot A, Helbling A, Petitot C, Ferrand C, Collin B, et al. IL-1RAP, a Key
730 Therapeutic Target in Cancer. Int J Mol Sci 2022;23.
731 39. Wesche H, Korherr C, Kracht M, Falk W, Resch K, Martin MU. The interleukin-1 receptor accessory
732 protein (IL-1RAcP) is essential for IL-1-induced activation of interleukin-1 receptor-associated kinase
733 (IRAK) and stress-activated protein kinases (SAP kinases). J Biol Chem 1997;272:7727-7731.
734 40. Greenfeder SA, Nunes P, Kwee L, Labow M, Chizzonite RA, Ju G. Molecular cloning and
735 characterization of a second subunit of the interleukin 1 receptor complex. J Biol Chem
736 1995;270:13757-13765.
737 41. Diaz-Guillen MA, Rodriguez de Cordoba S, Heine-Suner D. A radiation hybrid map of complement
738 factor H and factor H-related genes. Immunogenetics 1999;49:549-552.
739 42. Jozsi M, Meri S. Factor H-related proteins. Methods Mol Biol 2014;1100:225-236.
740 43. Wan Z, Li X, Luo X, Wang B, Zhou X, Chen A. The miR-590-3p/CFHR3/STAT3 signaling pathway
741 promotes cell proliferation and metastasis in hepatocellular carcinoma. Aging (Albany NY)
742 2022;14:5783-5799.
743 44. Mirea AM, Tack CJ, Chavakis T, Joosten LAB, Toonen EJM. IL-1 Family Cytokine Pathways
744 Underlying NAFLD: Towards New Treatment Strategies. Trends Mol Med 2018;24:458-471.
745 45. Tilg H, Effenberger M, Adolph TE. A role for IL-1 inhibitors in the treatment of non-alcoholic fatty
746 liver disease (NAFLD)? Expert Opin Investig Drugs 2020;29:103-106.
747 46. Gehrke N, Hofmann LJ, Straub BK, Ruhle F, Waisman A, Galle PR, Schattenberg JM. Hepatic
748 interleukin-1 receptor type 1 signalling regulates insulin sensitivity in the early phases of nonalcoholic
749 fatty liver disease. Clin Transl Med 2022;12:e1048.
750 47. He Y, Hwang S, Ahmed YA, Feng D, Li N, Ribeiro M, Lafdil F, et al. Immunopathobiology and
751 therapeutic targets related to cytokines in liver diseases. Cell Mol Immunol 2021;18:18-37.
752 48. Pan J, Ou Z, Cai C, Li P, Gong J, Ruan XZ, He K. Fatty acid activates NLRP3 inflammasomes in
753 mouse Kupffer cells through mitochondrial DNA release. Cell Immunol 2018;332:111-120.
754 49. Butler A, Hoffman P, Smibert P, Papalexi E, Satija R. Integrating single-cell transcriptomic data
755 across different conditions, technologies, and species. Nat Biotechnol 2018;36:411-420.
756 50. Tanino Y, Wang X, Nikaido T, Misa K, Sato Y, Togawa R, Kawamata T, et al. Syndecan-4 Inhibits the
757 Development of Pulmonary Fibrosis by Attenuating TGF-beta Signaling. Int J Mol Sci 2019;20.
758 51. Becsky D, Gyulai-Nagy S, Balind A, Horvath P, Dux L, Keller-Pinter A. Myoblast Migration and
759 Directional Persistence Affected by Syndecan-4-Mediated Tiam-1 Expression and Distribution. Int J
760 Mol Sci 2020;21.
761 52. Chronopoulos A, Thorpe SD, Cortes E, Lachowski D, Rice AJ, Mykuliak VV, Rog T, et al. Syndecan-4
762 tunes cell mechanics by activating the kindlin-integrin-RhoA pathway. Nat Mater 2020;19:669-678.
763 53. Lambert J, Makin K, Akbareian S, Johnson R, Alghamdi AAA, Robinson SD, Edwards DR.
764 ADAMTS-1 and syndecan-4 intersect in the regulation of cell migration and angiogenesis. J Cell Sci
765 2020;133.

766 54. Scheving LA, Zhang X, Threadgill DW, Russell WE. Hepatocyte ERBB3 and EGFR are required for
767 maximal CCl4-induced liver fibrosis. Am J Physiol Gastrointest Liver Physiol 2016;311:G807-G816.
768 55. Xiong J, Ni J, Chen C, Wang K. miR-148a-3p regulates alcoholic liver fibrosis through targeting
769 ERBB3. Int J Mol Med 2020;46:1003-1012.
770
771
772

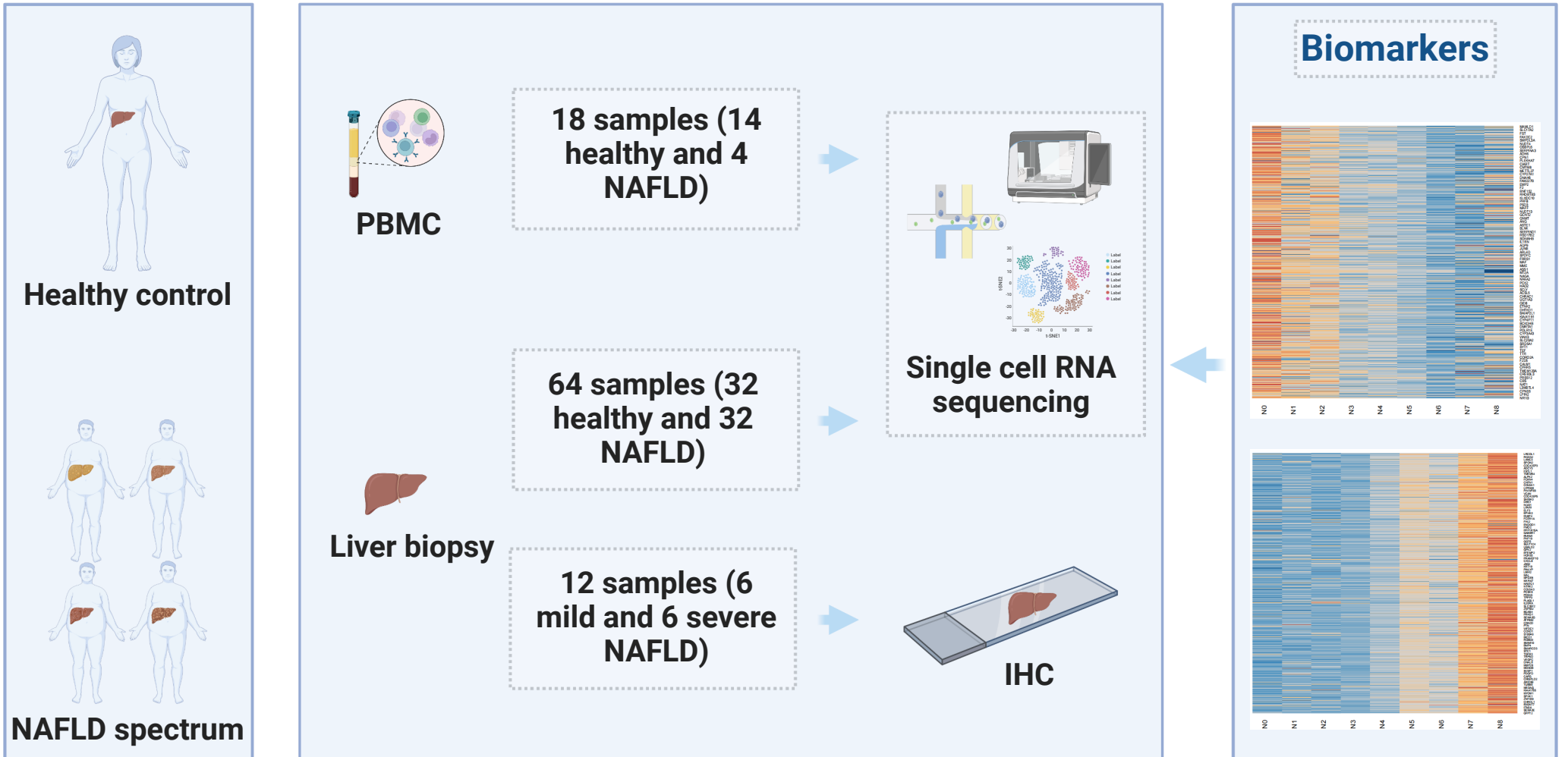
Healthy control
NAFLD spectrum
PBMC
Liver biopsy
18 samples (14 healthy and 4 NAFLD)
64 samples (32 healthy and 32 NAFLD)
12 samples (6 mild and 6 severe NAFLD)
Single cell RNA sequencing
IHC
Biomarkers
Created with BioRender.com

# Figure1

A

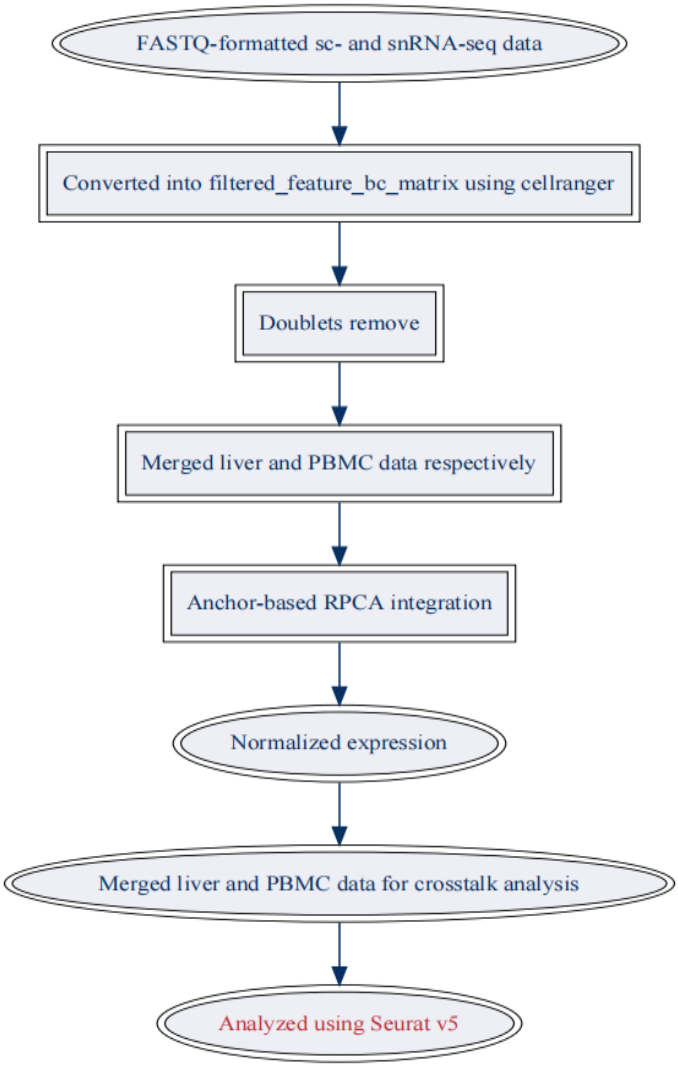


B

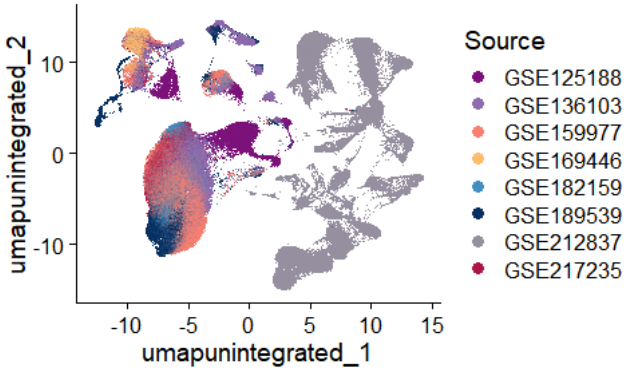


C

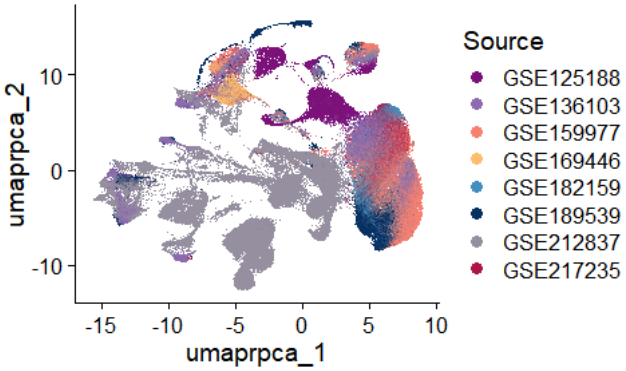


D

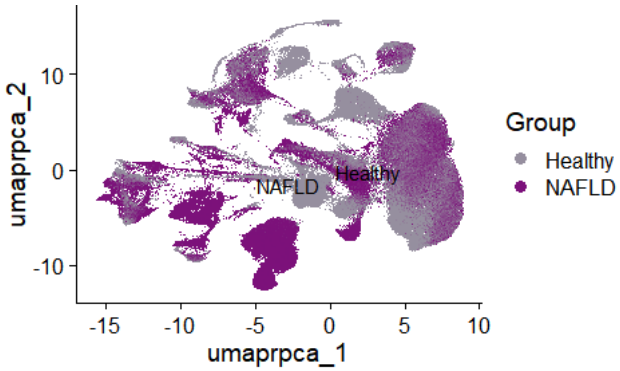


E

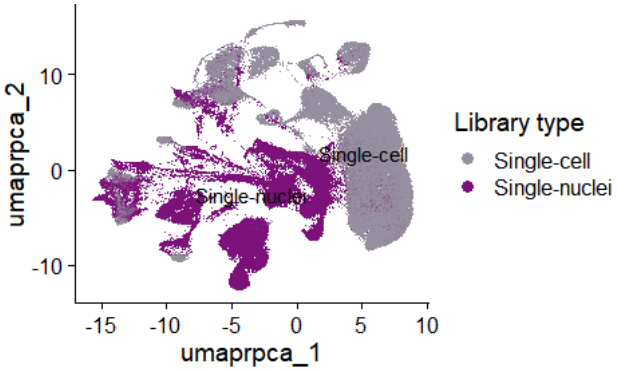


F

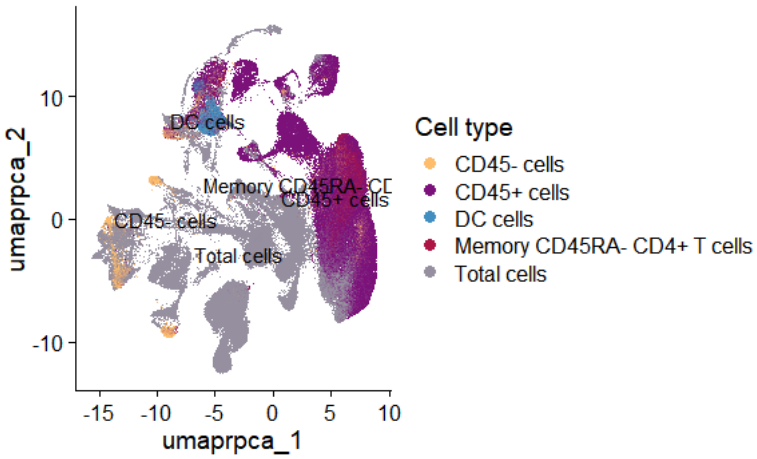

# Figure 2

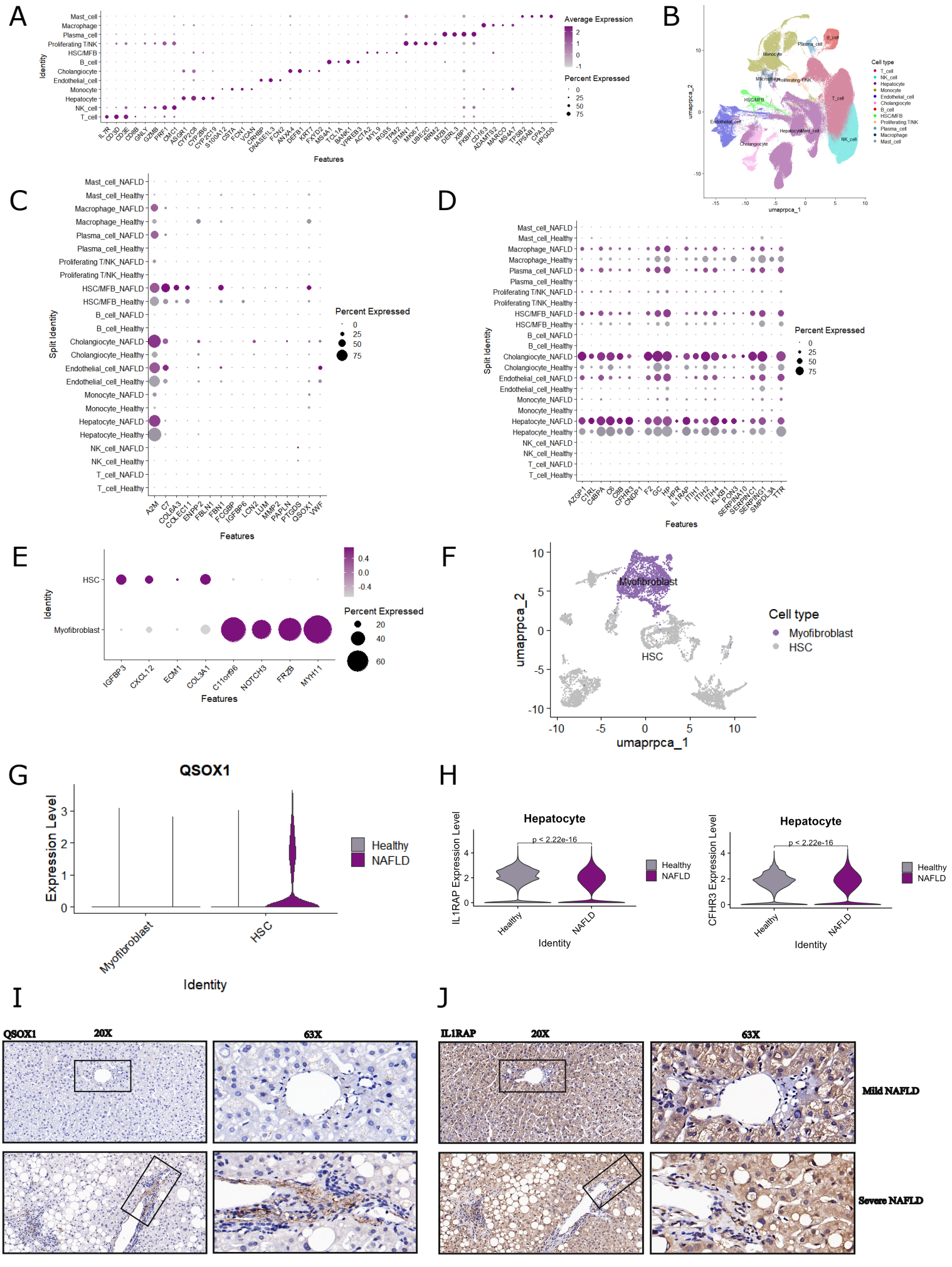
A
Mast_cell
Macrophage
Plasma_cell
Proliferating T/NK
HSC/MFB
B_cell
Cholangiocyte
Endothelial_cell
Monocyte
Hepatocyte
NK_cell
T_cell
Identity
Features
Average Expression
Percent Expressed
B
Cell type
T_cell
NK_cell
Hepatocyte
Monocyte
Endothelial_cell
Cholangiocyte
B_cell
HSC/MFB
Proliferating T/NK
Plasma_cell
Macrophage
Mast_cell
umaprrpca_1
umaprrpca_2
C
Mast_cell_NAFLD
Mast_cell_Healthy
Macrophage_NAFLD
Macrophage_Healthy
Plasma_cell_NAFLD
Plasma_cell_Healthy
Proliferating T/NK_NAFLD
Proliferating T/NK_Healthy
HSC/MFB_NAFLD
HSC/MFB_Healthy
B_cell_NAFLD
B_cell_Healthy
Cholangiocyte_NAFLD
Cholangiocyte_Healthy
Endothelial_cell_NAFLD
Endothelial_cell_Healthy
Monocyte_NAFLD
Monocyte_Healthy
Hepatocyte_NAFLD
Hepatocyte_Healthy
NK_cell_NAFLD
NK_cell_Healthy
T_cell_NAFLD
T_cell_Healthy
Split Identity
Features
Percent Expressed
D
Split Identity
Features
Percent Expressed
E
HSC
Myofibroblast
Identity
Features
Percent Expressed
F
Myofibroblast
HSC
Cell type
umaprrpca_1
umaprrpca_2
G
QSOX1
Expression Level
Healthy
NAFLD
Myofibroblast
HSC
Identity
H
Hepatocyte
IL1RAP Expression Level
CFHR3 Expression Level
p < 2.22e-16
Healthy
NAFLD
Identity
I
QSOX1
20X
63X
J
IL1RAP
20X
63X
Mild NAFLD
Severe NAFLD

# Figure 3

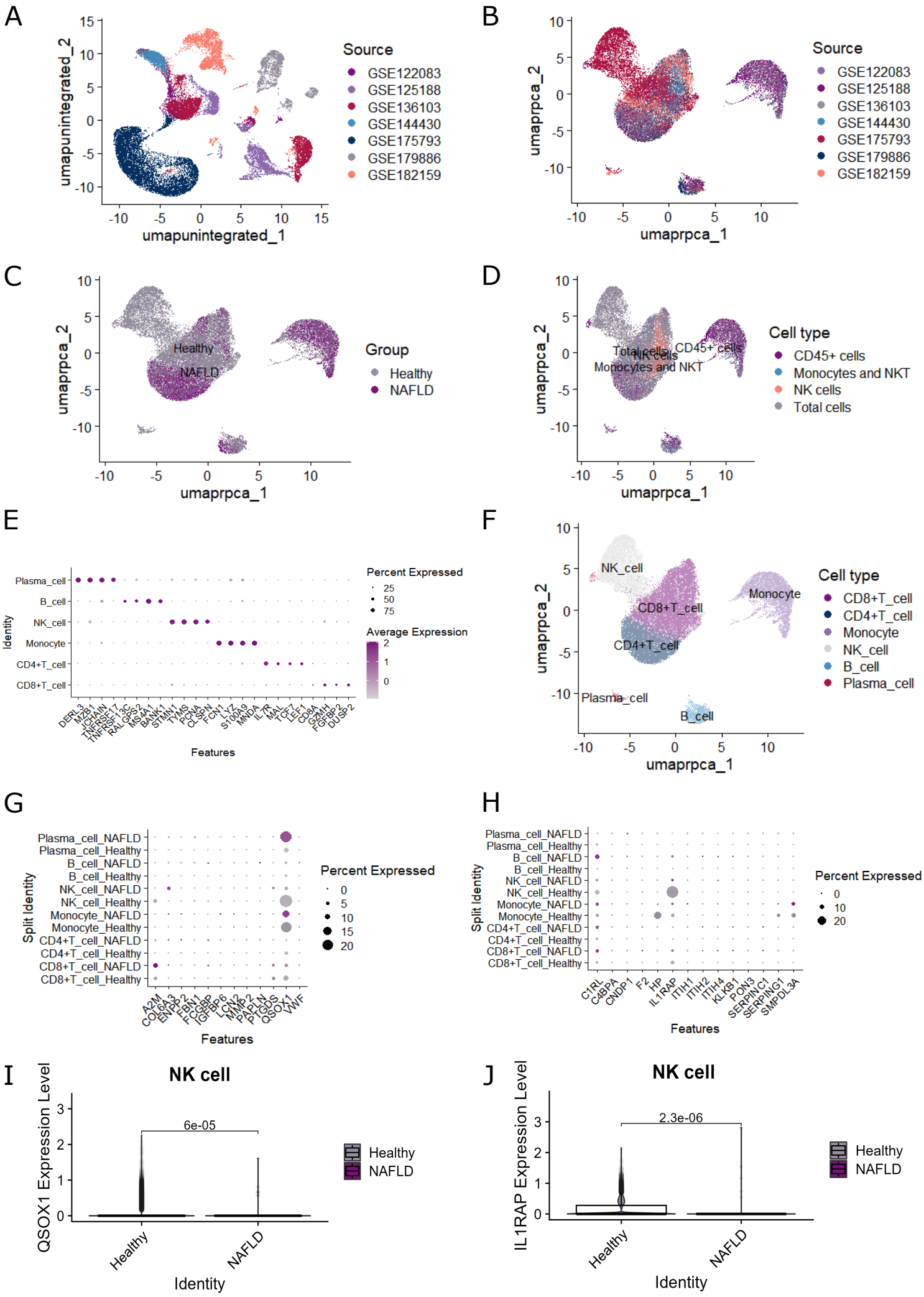
A
umapunintegrated_2
umapunintegrated_1
Source
GSE122083
GSE125188
GSE136103
GSE144430
GSE175793
GSE179886
GSE182159
B
umaprpca_2
umaprpca_1
Source
GSE122083
GSE125188
GSE136103
GSE144430
GSE175793
GSE179886
GSE182159
C
umaprpca_2
umaprpca_1
Healthy
NAFLD
Group
Healthy
NAFLD
D
umaprpca_2
umaprpca_1
Total cells
NK cells
CD45+ cells
Monocytes and NKT
Cell type
CD45+ cells
Monocytes and NKT
NK cells
Total cells
E
Plasma_cell
B_cell
NK_cell
Monocyte
CD4+T_cell
CD8+T_cell
Identity
DERL3
MZB1
HCHA1N
TNFRSF17
TNFRSF13C
RALGPS2
MS4A1
BANK1
STMN1
TYMS
PCNA
CLSPN
FCN1
LYZ
S100A9
MNDA
IL7R
MAL
TCF7
LEF1
CD8A
GZMH
FGFBP2
DUSP2
Features
Percent Expressed
25
50
75
Average Expression
2
1
0
F
umaprpca_2
umaprpca_1
NK_cell
CD8+T_cell
CD4+T_cell
Monocyte
Plasma_cell
B_cell
Cell type
CD8+T_cell
CD4+T_cell
Monocyte
NK_cell
B_cell
Plasma_cell
G
Plasma_cell_NAFLD
Plasma_cell_Healthy
B_cell_NAFLD
B_cell_Healthy
NK_cell_NAFLD
NK_cell_Healthy
Monocyte_NAFLD
Monocyte_Healthy
CD4+T_cell_NAFLD
CD4+T_cell_Healthy
CD8+T_cell_NAFLD
CD8+T_cell_Healthy
Split Identity
A2M
COL6A3
ENPP2
FBN1
FCGBP
IGFBP6
LCN2
MMP2
PAPLN
PTGDS
QSOX1
VWF
Features
Percent Expressed
0
5
10
15
20
H
Plasma_cell_NAFLD
Plasma_cell_Healthy
B_cell_NAFLD
B_cell_Healthy
NK_cell_NAFLD
NK_cell_Healthy
Monocyte_NAFLD
Monocyte_Healthy
CD4+T_cell_NAFLD
CD4+T_cell_Healthy
CD8+T_cell_NAFLD
CD8+T_cell_Healthy
Split Identity
C1RL
C4BPA
CNDP1
F2
HP
IL1RAP
ITIH1
ITIH2
ITIH4
KLKB1
PON3
SERPINC1
SERPING1
SMPDL3A
Features
Percent Expressed
0
10
20
I
NK cell
QSOX1 Expression Level
6e-05
Healthy
NAFLD
Identity
J
NK cell
IL1RAP Expression Level
2.3e-06
Healthy
NAFLD
Identity

# Figure 4

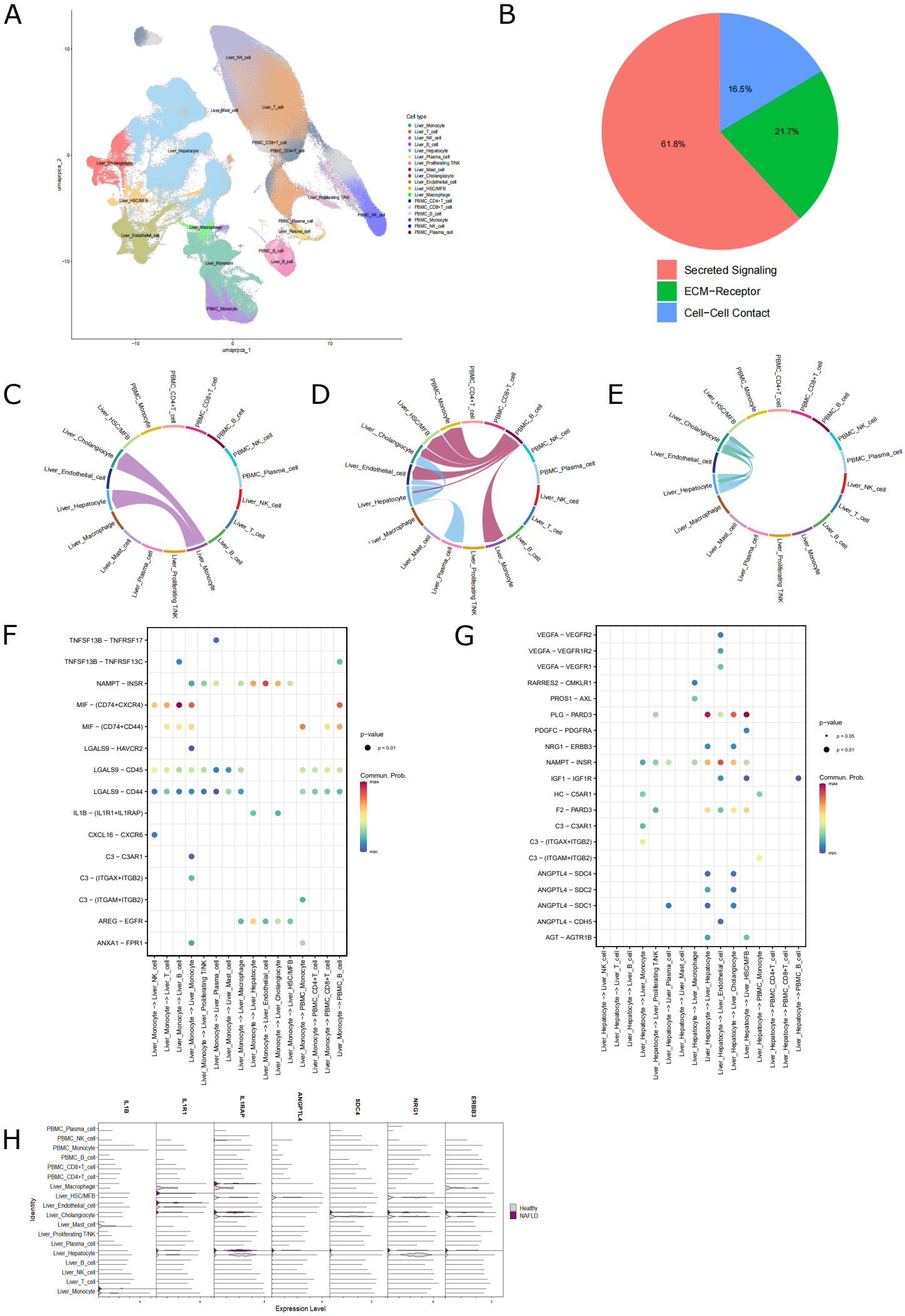
A
B
16.5%
21.7%
61.8%
Secreted Signaling
ECM−Receptor
Cell−Cell Contact
C
D
E
F
G
H
IL1B
IL1R1
IL1RAP
ANGPTL4
SDC4
NRG1
ERBB3
Expression Level
Healthy
NAFLD